Use of a pH-responsive imatinib mesylate sustained-release hydrogel for the treatment of tendon adhesion by inhibiting PDGFRβ/CLDN1 pathway

Sa Pang [a,1], Rongpu Wu [a,1], Wenxin Lv [b,1], Jian Zou [a,1], Yuange Li [a], Yanhao Li [a], Peilin Zhang [a], Xin Ma [a,***], Yi Wang [b,**], Shen Liu [a,*]

[a] Department of Orthopaedics, Shanghai Sixth People's Hospital Affiliated to Shanghai Jiao Tong University School of Medicine, 600 Yishan Rd, Shanghai, 200233, PR China
[b] Center for Advanced Low-dimension Materials, State Key Laboratory for Modification of Chemical Fibers and Polymer Materials, College of Chemistry and Chemical Engineering, Donghua University, Shanghai, 201620, PR China

ARTICLE INFO

ABSTRACT

Adhesion after tendon injury, which can result in limb movement disorders, is a common clinical complication; however, effective treatment methods are lacking. Hyaluronic acid hydrogels are a new biomedical material used to prevent tendon adhesion owing to their good biocompatibility. In addition, potential drugs that inhibit adhesion formation have gradually been discovered. The anti-adhesion effects of a combination of loaded drugs into hydrogels have become an emerging trend. However, current drug delivery systems usually lack specific regulation of drug release, and the effectiveness of drugs for treating tendon adhesions is mostly flawed. In this study, we identified a new drug, imatinib mesylate (IM), that prevents tendon adhesion and explored its related molecular pathways. In addition, we designed a pH-responsive sustained-release hydrogel for delivery. Using the metal-organic framework ZIF-8 as a drug carrier, we achieved controlled drug release to increase the effective drug dose at the peak of adhesion formation to achieve better therapeutic effects. The results showed that IM blocked the formation of peritendon adhesions by inhibiting the PDGFRβ/ERK/STAT3/CLDN1 pathway. Furthermore, the hydrogel with ZIF-8 exhibited better physical properties and drug release curves than the hydrogel loaded only with drugs, showing better prevention and treatment effects on tendon adhesion.

1. Introduction

Adhesion formation after tendon injury is a clinically significant tendon healing complication that can lead to functional disability [1,2]. It can be divided into three stages: inflammation, proliferation, and remodeling [3]. The proliferative phase, in which the synthesis of type III collagen reaches its peak, mainly comprises adhesion formation [4,5]. A hydrogel is a physical barrier used to prevent or limit tendon adhesion [6]. Loading drugs through the hydrogel to inhibit the growth of adhesion tissue is a common strategy [7]. However, for some currently constructed drug-loaded hydrogel materials, the rate of drug release from the hydrogel is too fast, with a cumulative release of nearly 80 % within 7 days [8]. Therefore, the current drug-loaded hydrogel

material releases less drug during the peak period of adhesion tissue synthesis, that is, the proliferative stage of tendon healing, which results in this barrier being less effective in inhibiting tendon adhesion than expected. To address this issue, novel drug-loaded hydrogels aim to reduce the drug release rate and prolong the drug release time, thereby increasing the effective amount of drug the hydrogel can release during the proliferative phase of adhesion formation.

ZIFs are metal-organic frameworks (MOF) that have high thermal and hydrothermal stability [9]. The ZIFs are used as carriers for metal nanoparticles and drugs [10–12]. ZIF-8 is a non-toxic and biocompatible ZIF composed of zinc ions and 2-methylimidazolate [13]. pH-sensitive drug delivery systems can be constructed using ZIF-8, as it is stable under physiological conditions and decomposes under acidic conditions

---

[14–16]. Experiments have confirmed that local lactate synthesis increases sharply 1 week after tendon injury [17], and increased lactate production is also observed 4 weeks after injury [18]. Therefore, the use of ZIF-8 as a drug carrier may extend the time of drugs released from hydrogels. In addition, there is the possibility that the drug can be slowly released in the acidic environment around the site of tendon injury to achieve on-demand inhibition of adhesion formation around the tendons.

Drugs currently used to treat tendon adhesion, such as corticosteroids [19], non-steroidal anti-inflammatory drugs [20], and core proteoglycans [21], have either unsatisfactory anti-adhesion effects or side effects, such as poor tendon healing [22–24]. Therefore, finding a potential anti-adhesion drug that not only has a good inhibitory effect on tendon adhesion but also has the smallest possible impact on the process of tendon healing is crucial. Imatinib mesylate (IM) is a small-molecule anti-cancer drug that specifically inhibits several protein tyrosine kinases, including Abl, Arg, platelet-derived growth factor receptor (PDGFR), and its carcinogenic form [25]. Studies have confirmed the inhibitory effects of IM on pulmonary fibrosis [26], liver fibrosis [27], and systemic sclerosis [28]. Adhesion during tendon regeneration results from interactions between inflammatory cells and local ischemia [29]. Platelet-derived growth factor (PDGF) is a key cytokine in this process, which not only stimulates the differentiation and proliferation of myofibroblasts but also stimulates excessive deposition of collagen protein [30]. IM can selectively inhibit PDGFR [28], which may also be the mechanism by which IM inhibits tendon adhesion.

HA is a biodegradable, biocompatible, and non-toxic natural polymer [31]. HA, which stimulates angiogenesis and reduces inflammation [32], has been used to fabricate injectable hydrogels in biomedicine [33]. HA hydrogels are classic anti-adhesion biomaterials. It is an important source of nutrition and lubricant for tendon sliding. Furthermore, owing to its negative charge, HA can inhibit the growth of fibroblasts, cell proliferation, migration, and adhesion [3]. However, its special three-dimensional structure enables it to slowly release the inner material by regulating the decomposition rate of the degradable outer hydrophobic groups [34]. Owing to this property, it can be used as a drug carrier [35], in addition to a dressing for injured tendons; on the one hand, it controls the release of drugs, and on the other hand, it inhibits the formation of adhesion tissue at the physical level.

In this study, we screened IM, an effective drug that inhibits myofibroblasts proliferation and collagen secretion, and designed a MOF-based hydrogel loaded with a drug to prevent tendon adhesion. The main steps were as follows: Based on the results of the drug chip, we screened and verified possible drugs that inhibit fibroblasts. We selected IM, which had the best effect and synthesized IM@ZIF-8, *N*-carboxyethyl chitosan (CEC), and oxidized hyaluronic acid (OHA). The required amount of IM@ZIF-8 was pre-dissolved in the OHA solution, and the OHA solution and biocompatible polymer CEC solutions were mixed. Schiff base bonds formed under physiological conditions to prepare drug-loaded hydrogels [36]. We speculate that IM can inhibit the formation of adhesion tissue by inhibiting the proliferation and collagen secretion of myofibroblasts, while ZIF-8 can slow down the release of the drug into the tendon microenvironment, thus allowing more drug in the adhesion tissue. The peak of formation takes effect, while the hydrogel acts as a physical barrier that prevents adhesion tissue from invading the tendon.

2. Result

2.1. Preparation and characterization of IM@ZIF-8

In this study, ZIF-8 was synthesized using $Zn(CH_3COO)_2 \cdot 2H_2O$ and 2-methylimidazole, while ZIF-8 loaded with IM was synthesized employing a one-pot method. Zinc coordinated with IM to generate a coordination polymer, and MOFs were formed through the addition of organic ligands and metal ions. During this process, IM was encapsulated to form

the IM@ZIF-8 MOF (Fig. 1a). The representative surface morphology shows that they have the same cubic structure, and IM@ZIF-8, due to drug loading, has a larger volume than that of ZIF-8 alone (Fig. 1b).

2.2. Preparation and characterization of hydrogel

OHA and CEC solutions were mixed under physiological conditions to produce hydrogels. The molecular formulas of OHA and CEC are shown in Fig. S1. They were crosslinked by the formation of a Schiff base bond between the amino group of CEC and the residual aldehyde group of OHA (Fig. 1c). The purified OHA, CEC, and gel products were confirmed by Fourier-transform infrared spectroscopy (FTIR). FITR gel exhibited a strong peak at 1678 cm^{-1}, corresponding to the Schiff base formed between OHA and CEC (Fig. 1d). Finally, the synthesis of IM@ZIF-8@Gel was achieved by combining IM@ZIF-8 with the CEC solution and mixing it with OHA. We detected the representative surface morphologies of these two types of gels using scanning electron microscopy (SEM), and the results showed that IM@ZIF-8@Gel had the same morphology and pore size as the pure gels, but the difference was the addition of IM@ZIF-8 attached to the gel (Fig. 1f). We also conducted biomechanical testing, and it was found that the maximum load and elastic modulus of the gel were higher than Gel alone when IM@ZIF-8 was added (Fig. 1e), indicating that the presence of MOFs increased the biomechanical strength of the gel. By measuring the storage modulus (G′) and loss modulus (G″) of the hydrogel at a fixed frequency (1 rad s^{-1}), we explored the rheological properties of the IM@ZIF-8@Gel hydrogel. Pure gels had the highest storage modulus of all the hydrogels. With the addition of ZIF-8, the G′ of the gel decreased (Fig. 1g). The drug release rate indicates that in the IM@ZIF-8@Gel, compared to IM@Gel, the release of drugs is slower. On day 8, nearly 80 % of the medication was released by the IM@Gel, compared to the IM@ZIF-8@Gel, which released <50 %. Therefore, during the peak period of collagen formation, which is 7–21 days, drug release with the IM@ZIF-8@Gel was significantly higher than with the IM@Gel (Fig. 1h).

2.3. Drug screening and mechanism detection

2.3.1. Potential drug screening

By consulting papers related to fibrosis, we screened 12 potential anti-tendon adhesion drugs, including IM, that could inhibit fibroblast proliferation. We further screened these 12 drugs by detecting their effects on the proliferation of 208f rat fibroblasts and TDSC rat tendon stem cells using the cell counting kit 8 (CCK-8). We co-cultured 12 drugs with two types of cells, and after 3 days, we conducted a statistical analysis using the CCK8 assay. It was found that IM significantly inhibited fibroblast proliferation, whereas its inhibitory effect on tendon stem cells was relatively weak (Fig. 2a). Therefore, IM was chosen as a potentially effective drug for the treatment of tendon adhesions in subsequent experiments.

2.3.2. Mechanism of IM inhibition of fibrosis

To further investigate the specific mechanisms involved in the inhibition of fibroblast proliferation by IM, we conducted RNA-Seq on fibroblasts co-cultured with IM for 3 days (the control group had the same volume of solvent without IM). We found that there was a significant decrease in adhesion pathway expression in both GO and KEGG analyses (Fig. 2b and c). Through the analysis of sequencing results, we conducted differential gene screening, analyzed the top 50 genes (Fig. 2d), identified the genes closely related to fibrosis, and ultimately located *CLDN1*. From the sequencing results compared to the control group, the expression of *CLDN1* in fibroblasts co-cultured with IM was significantly decreased. Therefore, we speculate that IM inhibits fibrosis by reducing the expression of *CLDN1*.

2.3.3. Relationship between CLDN1 and peritendinous adhesion

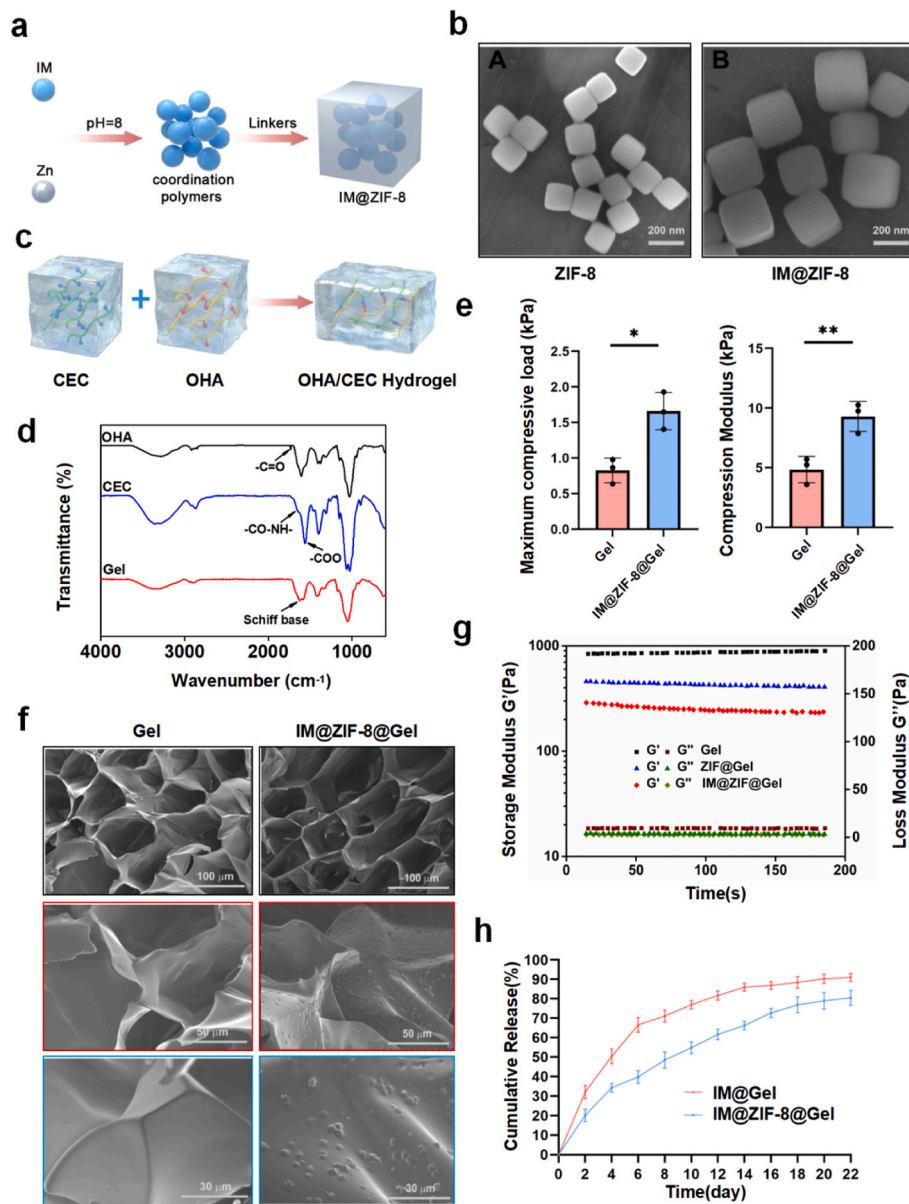To elucidate the association between CLDN1 and tendon adhesion,

Fig. 1. Characterization of different ZIF-8 and gels. a) Schematic diagram of IM@ZIF-8 synthesis. b) Scanning electron microscope (SEM) macrographs of ZIF-8 and IM@ZIF-8. c) Molecular formula of OHA/CEC hydrogel synthesis. d) FT-IR spectra of the CEC polymer, OHA polymer, and OHA/CEC gel. e) Maximum compressive stress and compression modulus of the Gel and IM@ZIF-8@Gel (mean ± SD, *P < 0.05, **P < 0.01, ***P < 0.001, n = 3). f) SEM macrographs of the Gel and IM@ZIF-8@Gel. g) Rheological properties of the Gel, ZIF-8@Gel, and IM@ZIF-8@Gel. h) Drug release curve of IM@Gel and IM@ZIF-8@Gel at pH 6.

we used Kessler sutures to simulate tendon repair in the experimental group of mice with severed flexor digitorum profundus tendons, whereas the control group did not undergo surgical treatment. Tissue samples were harvested on the 14th postoperative day, and immunohistochemical staining was used to analyze the density and location of CLDN1 in the peritendinous tissue (Fig. 3a). The results showed that, compared to normal peritendinous tissue, the expression of CLDN1 was significantly increased in the adhesive tissue formed after injury (Fig. 3b).

2.3.4. Expression of PDGFR in human adhesive tissues

Samples of normal peritendinous tissue and peritendinous adhesive tissue were obtained from patients undergoing tendon repair surgery, followed by single-cell sequencing to analyze the two subtypes, PDGFRα and PDGFRβ. The distribution and strength of PDGFRα and PDGFRβ in adhesive tissue were observed. They are mainly expressed in fibroblasts; However, PDGFRβ is distributed in almost all fibroblasts, while PDGFRα

is only expressed in some fibroblasts. Compared to the normal group, the expression of PDGFRβ increased significantly in the peritendinous tissue 10 days after injury, while PDGFRα showed no significant increase (Fig. 3c and d). These results indicate that PDGFRβ may be more closely related to the formation of adhesive tissue.

2.3.5. PDGFRβ regulating the expression of CLDN1

To investigate the mechanism of IM inhibition of CLDN1, we investigated the effects of SU16f (a selective PDGFRβ inhibitor). Western blotting was used to validate the expression of PDGFRβ in myofibroblasts co-cultured with the inhibitor and control solvent groups for 3 days (Fig. 3e). The expression of ERK1/2, p-ERK1/2, STAT3, p-STAT3, and CLDN1 were assessed (Fig. 3f–i). The results indicate that SU16f can inhibit PDGFRβ phosphorylation, which resulted in a significant reduction in the phosphorylation of ERK1/2 and STAT3, while the expression of CLDN1 decreased.
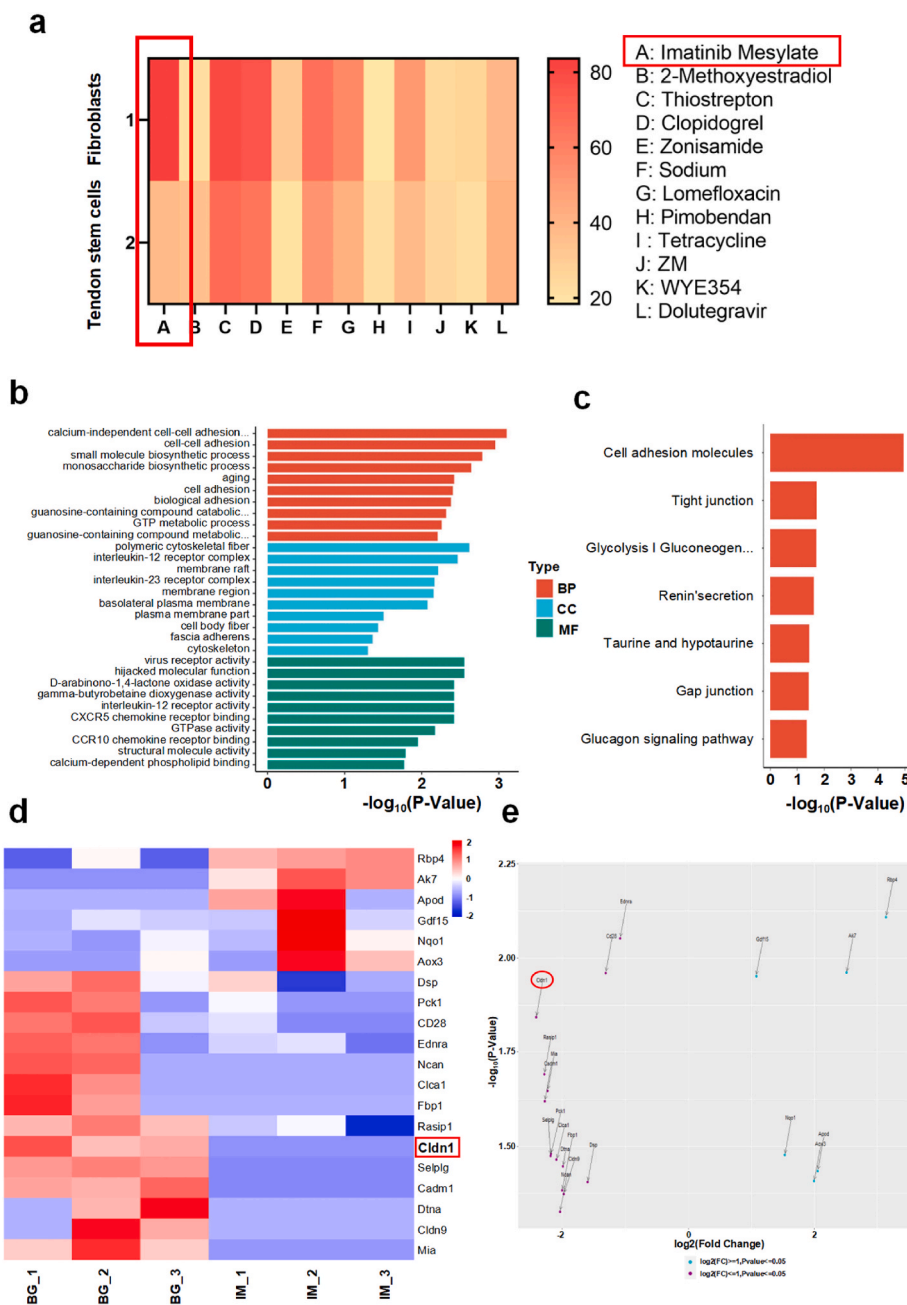
Fig. 2. Screening of drugs and research on their mechanisms of action. a) Heat map of the inhibition rate of different drugs on fibroblasts and tendon stem cells. b) p-value bar plot of the top Gene Ontology (GO) enrichment terms. c) p-value bar plot of Kyoto Encyclopedia of Genes and Genomes (KEGG) enrichment analysis. d) Heat map of differentially expressed genes related to fibrosis. e) Volcano plot of differentially expressed genes related to fibrosis.

2.4. In vitro experiment of drug-loaded hydrogel

2.4.1. Screening of loaded drug concentrations

Based on preliminary calculations, we constructed three drug-loaded gel concentrations. To determine the optimal concentration, we collected the aqueous extracts of the three concentrations of drug-loaded hydrogel and the hydrogel containing only nanoparticles for 7–14 days, co-cultured them with myofibroblasts and tendon stem cells, and counted them using CCK8 assay 3 days later. The results showed that the 0.26 mg/mL drug-loaded gel had a more significant inhibitory effect on myofibroblast proliferation than the other two hydrogel concentrations, whereas the inhibitory effect on tendon stem cells was not significantly increased (Fig. 4b and c). Therefore, we chose the 0.26 mg/mL concentration of drug-loaded hydrogel for further experiments.

2.4.2. Drug-loaded hydrogel inhibits the proliferation and adhesion of myofibroblasts

Cells with IM@ZIF-8@Gels and the pure drug-carrying hydrogel IM@Gel were assessed using live/dead staining, ghost pen staining, and the CCK8 counting kit. The effect of anti-adhesion and cytotoxicity on myofibroblasts was different, and ZIF@Gel group A served as the control group. The CCK8 assay showed that the pure hydrogel and the nanoparticles themselves have no effect on the proliferation of myofibroblasts. The IM@ZIF-8@Gel group showed stronger inhibitory effects on myofibroblasts after co-culturing with myofibroblasts for 1, 3, and 5 days compared to the IM@Gel group (Fig. 4d, e, f). Staining and statistical analysis of dead/living cells revealed a significant difference in myofibroblasts cytotoxicity on day 3, where the IM@ZIF-8@Gel group showed stronger cytotoxicity (Fig. 4h and i). In addition to the
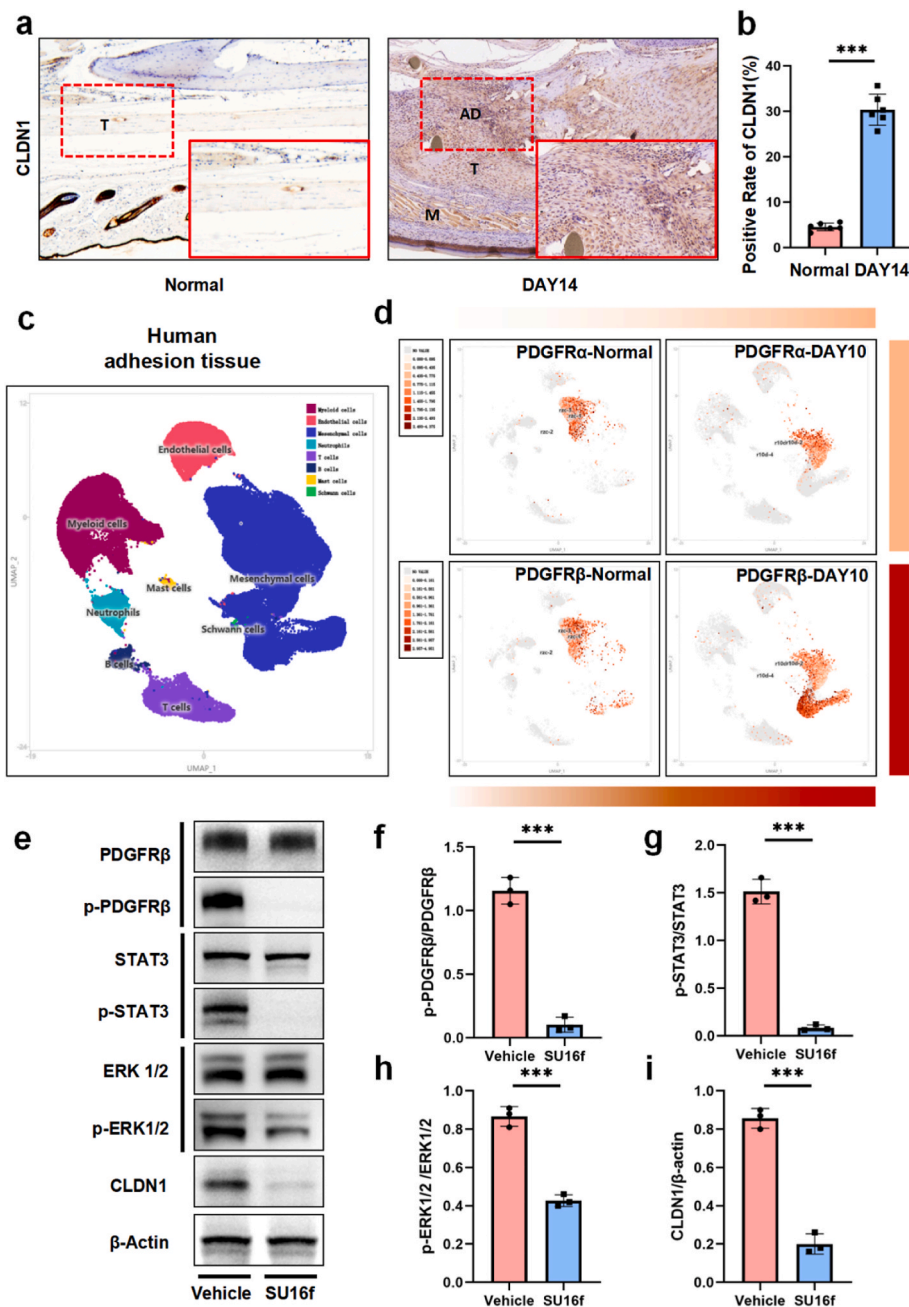
Fig. 3. Protein expression in vivo. a. b) Immunohistochemical staining and evaluation of CLDN1 expression in tendons of normal mice and injured mouse after 14 days of modeling (mean ± SD, *P < 0.05, **P < 0.01, ***P < 0.001, n = 6). c. d) Expression and distribution of PDGFRα and PDGFRβ in single-cell sequencing of normal human tissue and adhesive tissue at 10 days after surgery. e) Use Western blotting to detect protein expression in the cells co cultured with SU16f for 3 days. f) *p*-PDGFRβ expression normalized to PDGFRβ expression. g)p-STAT3 expression normalized to STAT3 expression. h) *p*-ERK1/2 expression normalized to ERK1/2 expression. i) CLDN1 expression normalized to β-actin expression (mean ± SD, *P < 0.05, **P < 0.01, ***P < 0.001, n = 3).

proliferative activity of myofibroblasts, we tested the effect of the drug-loaded hydrogel on the adhesion ability of myofibroblasts, which were then co-cultured with the extract of each group of hydrogels for 3 days, and the cytoskeleton was stained with ghost pen cyclic peptide (Fig. 5a). The results showed that ZIF-8@Gel myofibroblasts have good skeletal arrangement and ductility, whereas in the IM@Gel and IM@ZIF-8@Gel groups, the cell area of the gels that make up fibrous cells was significantly reduced, and relative to the IM@Gel group, the cell area was smaller in the IM@ZIF-8@Gel group (Fig. 5b). In summary, IM released from the drug-loaded gel can inhibit the proliferation and adhesion of myofibroblasts. The ZIF-8 framework can reduce the speed of IM release from the hydrogel. The gel and ZIF-8 had no effect on cell proliferation and activity.

2.4.3. Protein expression

In order to determine the effect of IM on myofibroblasts protein expression, we measured the expression of Col III, ERK1/2, *p*-ERK1/2, STAT3, p-STAT3, and CLDN1 in myofibroblasts. Protein blotting was performed on myofibroblasts co-cultured with the aforementioned gels for 3 days (Fig. 5c). In comparison with the other three groups, the expression of Col III, *p*-ERK1/2, p-STAT3, and CLDN1 was significantly decreased in the IM@Gel and IM@ZIF-8@Gel groups (Fig. 5d–g). Therefore, IM reduced the secretion of Col III, inhibited ERK1/2 and STAT3 phosphorylation, and downregulated downstream CLDN1.
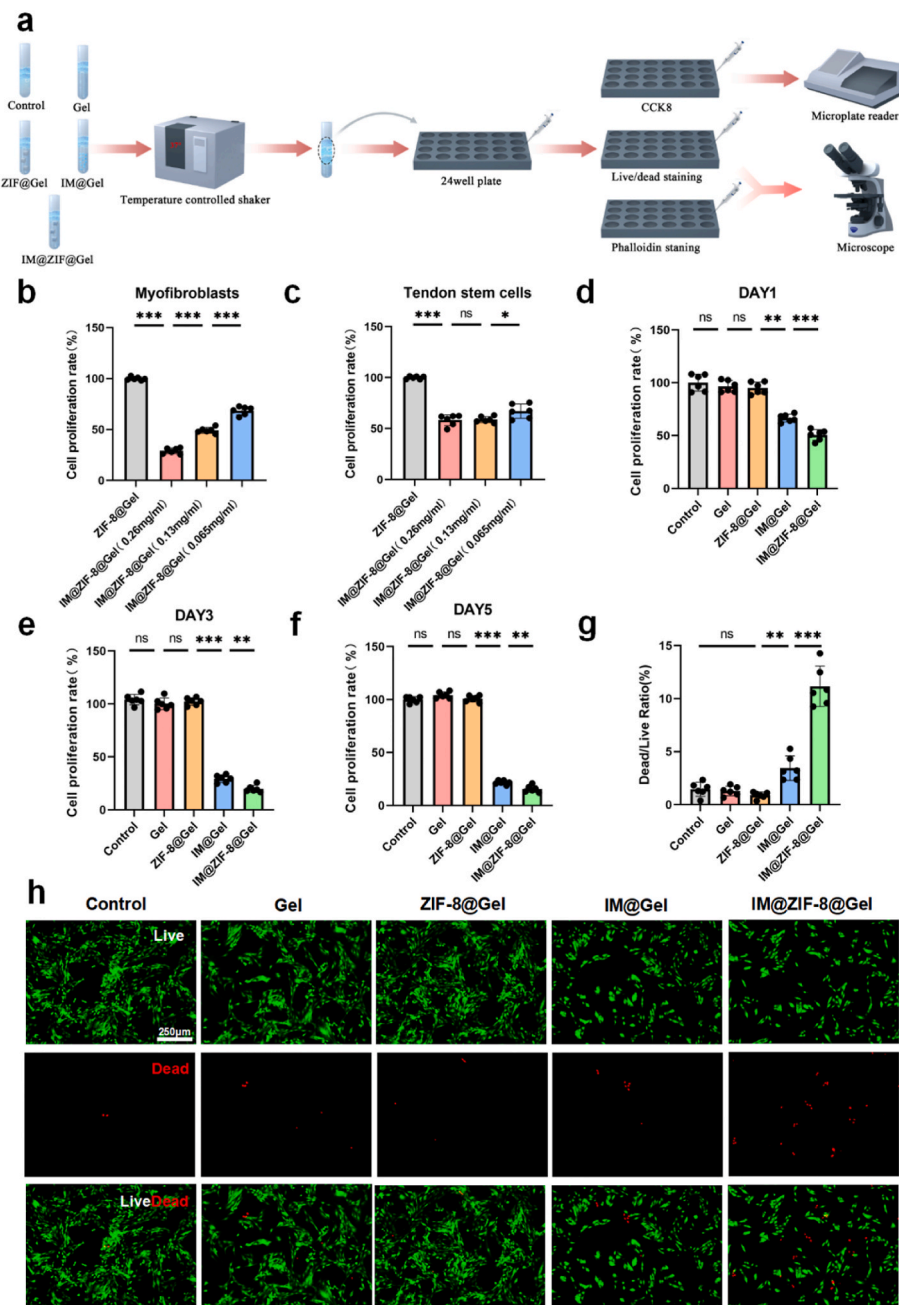
Fig. 4. Selection of the drug-loading concentration of hydrogel and its ability to inhibit myofibroblasts proliferation in vitro. a) The experimental process of evaluating myofibroblasts proliferation and adhesion in vitro. b,c) The CCK8 assay was used to analyze the effect of co-culture with different concentrations of hydrogel extracts on the proliferation of myofibroblasts and tendon stem cells for 3 days. d,e,f) The CCK8 assay was used to analyze the proliferation ability of myofibroblasts co-cultured with different hydrogel extracts on day 1, 3, and 5. h,i) myofibroblasts co-cultured with different hydrogel extracts for 3 days were stained alive/dead. Red: Dead cells; Green: Live cells (mean $\pm$ SD, *$p < 0.05$, * *$p < 0.01$, * * *$p < 0.001$, n = 6).

2.5. In vivo experiment of drug-loaded hydrogel

2.5.1. General observations and grading In vivo

We divided the rats into five groups: control group, Gel group, ZIF-8@Gel group, IM@Gel group, and IM@ZIF-8@Gel group; the control group was established as the rat Achilles tendon adhesion model without any hydrogel or medication. The surgical procedure for the tendon adhesion model is shown in Fig. 6a. After 21 days, all rats were euthanized, the area where the tendon was repaired was uncovered, and the attachment around the tendon was clearly visible. The number of adhesive tissues formed around the tendon and whether ion stripping could be used to separate the adhesive sites were scored. The results

showed that in the control group, the collagen fibers were tightly wrapped around the tendon, and it was difficult to separate the adhesive sites using ion stripping. The adhesive tissue in the Gel and ZIF-8 groups was slightly reduced, and after using the ion stripping force, the adhesive site could be slightly penetrated, whereas in the control group, IM@Gel group, and IM@ZIF-8@Gel group, the adhesive sites could be easily separated using stripping ions. Furthermore, compared to the IM@Gel group, there was less adhesive tissue on the surface of the tendon in the IM@ZIF-8@Gel group (Fig. 6b). The adhesion score in the IM@ZIF-8@Gel group was significantly lower than that of the other four groups (Fig. 6e).
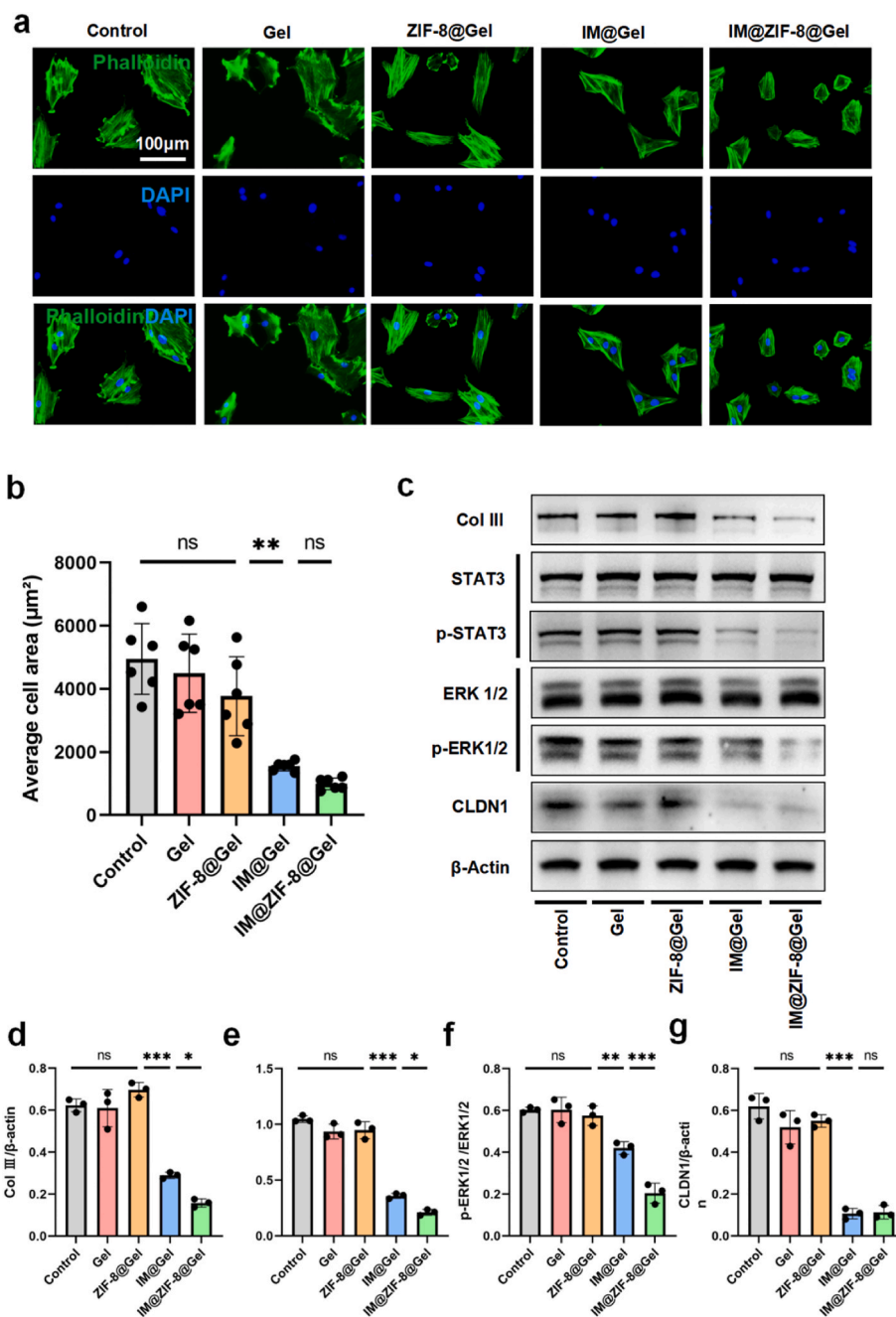
Fig. 5. Evaluation of hydrogels in vitro. a. b) Phalloidin staining of cytoskeleton and analysis of cell arrangement area of myofibroblasts co cultured with different groups of hydrogel release solution for 3 days (mean ± SD, *P < 0.05, * *P < 0.01, * *P < 0.001, n = 6). c) Use Western blotting to detect protein expression in the cells co cultured for 3 days.d) Col III expression normalized to β-actin expression. e) p-STAT3 expression normalized to STAT3 expression.f) *p*-ERK1/2 expression normalized to ERK1/2 expression.g) CLDN1 expression normalized to β-actin expression (mean ± SD, *P < 0.05, **P < 0.01, ***P < 0.001, n = 3).

2.5.2. *In vivo histological evaluation*

For the histological analysis of adhesion formation, all animal model specimens were stained with hematoxylin, eosin, and Masson's trichrome (Fig. 6c and d). An adhesion scoring system was used to evaluate the level of adhesion around the tendons, with higher scores indicating greater adhesive tissue formation around the tendons. The score in the IM@ZIF-8@Gel group was significantly lower than that in the other four groups (Fig. 6f and g). Besides, the basic structures of the major organs were normal. No indications of inflammatory cell infiltration or cell death or injury were detected, suggesting good systemic biocompatibility of IM@ZIF-8@Gel (Fig. S18).

2.5.3. *Evaluation of tendon healing*

We used a healing scoring system and biomechanical analysis to evaluate the effect of the drug-loaded hydrogel on tendon healing. The higher the healing score and maximum tensile strength of the tendon, the better the tendon healing. Regarding the Gel group, ZIF-8@Gel group, IM@Gel group, and the IM@ZIF-8@Gel, the healing score and maximum tensile strength of the tendon in the Gel group were no statistical difference with the control group (Fig. 6h and i), indicating that IM and ZIF-8 had no adverse effect on tendon healing.

2.5.4. *Col III sedimentary analysis*

The density and location of Col III in adherent tissues were analyzed using immunohistochemical staining (Fig. 7a). The Col III fibers were
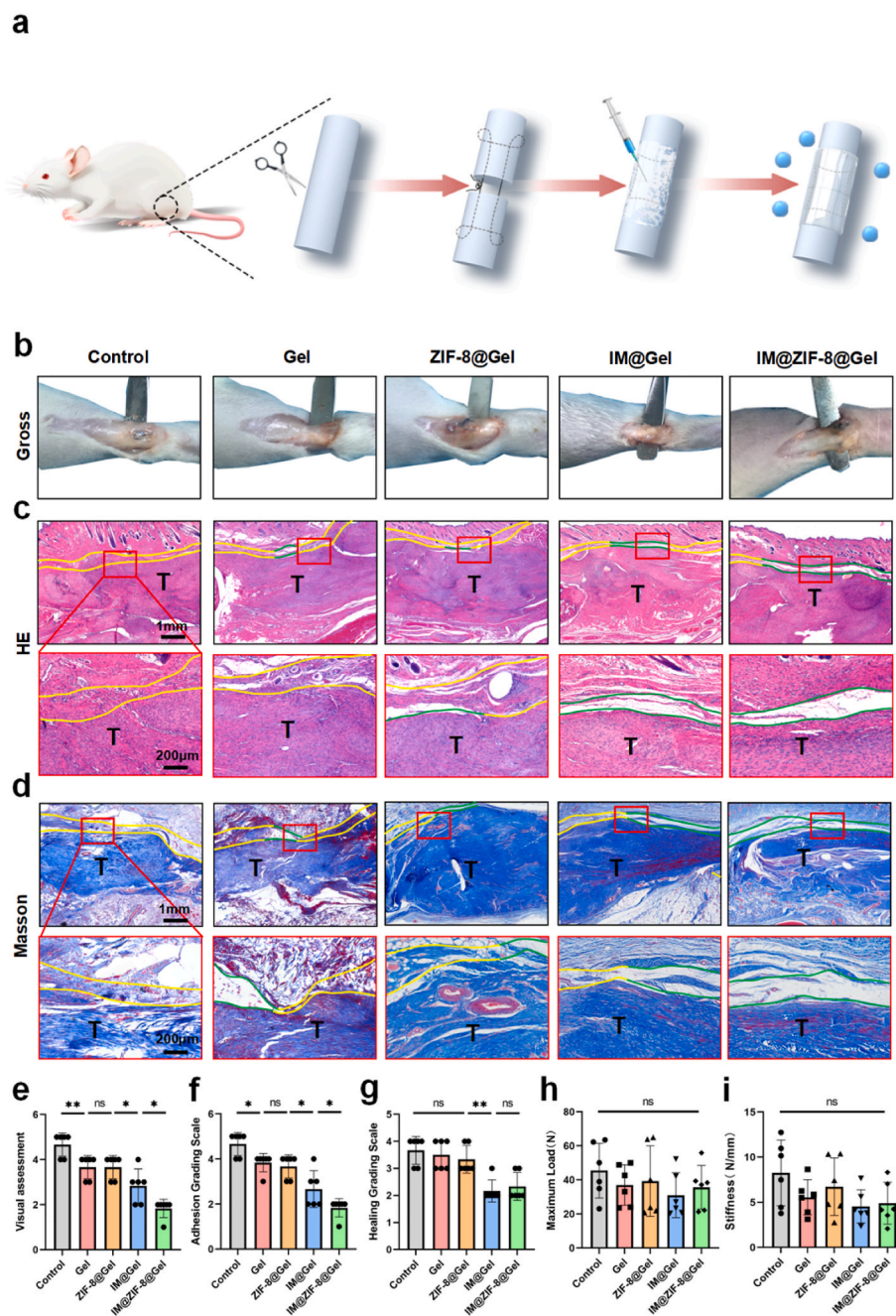
Fig. 6. Evaluation of the effect of different groups of hydrogels on the formation of peritendon adhesion. a) Schematic diagram of animal experiments. b) Gross observation of peritendinous adhesions. c) Comparison of gross scores of adhesion. d,e) Hematoxylin-eosin staining and Masson trichrome staining of different groups of Gel. Yellow liness indicate adhesion areas, and green lines indicate areas without adhesion. f) Comparison of histological scores for peritendinous adhesions. g) Comparison of histological scores for tendon healing. h) The maximum tensile strength of the repaired tendon. i) Repair the stiffness of the tendon (mean $\pm$ SD, *P < 0.05, **P < 0.01, ***P < 0.001, n = 6).

tinted in a shade of brown-yellow. The expression of Col III in the adhesive tissue of the IM@Gel group and IM@ZIF-8@Gel group was lower than that of the other three groups (Fig. 7b).

2.5.5. Protein expression in peritendinous tissue

Consistent with the results of the cytological analysis, protein blotting was used to confirm the expression of Col III, ERK1/2, *p*-ERK1/2, STAT3, p-STAT3, and CLDN1 in the adhesive tissues (Fig. 7c). The expression of Col III, *p*-ERK1/2, p-STAT3, and CLDN1 in the IM@Gel and IM@ZIF-8@Gel group was significantly lower than that in the other three groups (Fig. 7d–g, Fig. S17), indicating that IM reduced the secretion of Col III in vivo, inhibited the phosphorylation of ERK1/2 and

STAT3, and downregulated downstream CLDN1.

3. Discussion

The formation of peripheral adhesion during the repair of tendon injuries can seriously damage limb function [37]. In recent years, drug-loaded hydrogels have become a popular material for treating adhesion around tendons after injury [38]. We developed a sustained-release IM hydrogel delivery system with a pH-sensitive function. With the increase in lactic acid in the microcirculation after tendon injury, IM can be slowly released from ZIF-8 under acidic conditions. In addition, IM inhibited myofibroblasts proliferation and
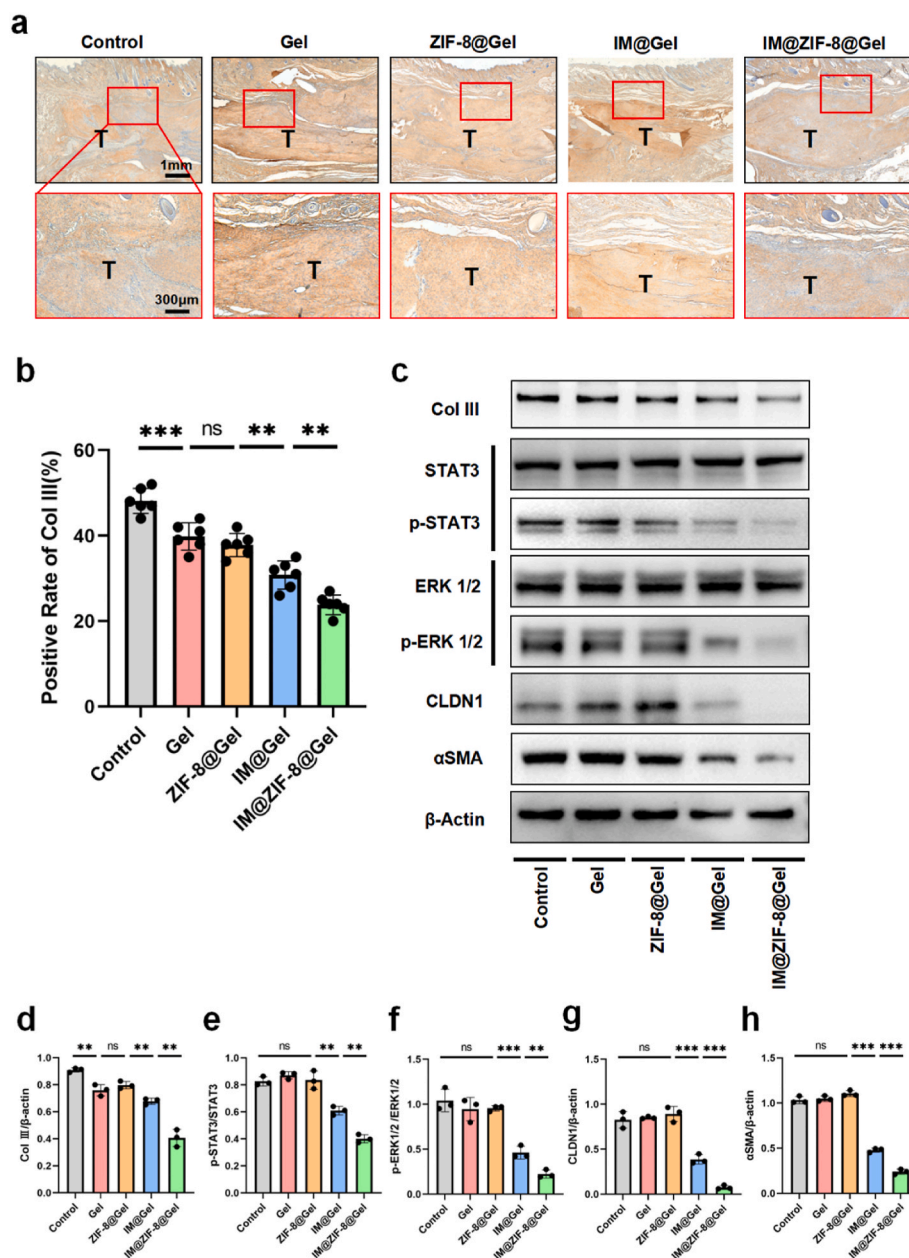
Fig. 7. Protein expression in vivo. a,b) Immunohistochemical staining and evaluation of Col III expression in adhesion area (mean ± SD, *P < 0.05, **P < 0.01, n = 6). c) Protein expressions in adhesion tissue were detected by Western Blot. d) Col III expression normalized to β-actin expression. e) p-STAT3 expression normalized to STAT3 expression. f) *p*-ERK1/2 expression normalized to ERK1/2 expression. g) CLDN1 expression normalized to β-actin expression. h) αSMA expression normalized to β-actin expression. (mean ± SD, *P < 0.05, **P < 0.01, ***P < 0.001, n = 3).

collagen secretion in vitro. When the hydrogel was applied to the damaged tendon, IM played an anti-adhesion role by blocking the PDGFRβ/ERK/STAT3/CLDN1 pathway without significantly preventing tendon healing.

Recent research has concentrated on the characteristics of hydrogels when it comes to drug release. Drug release is usually influenced by drug molecular weight, drug solubility, fiber material degradation rate, and other controlled-release strategies. There are both thermosensitive and small-molecule-responsive hydrogels [39]. However, the relevant hydrogels contain drugs or effective molecules that are directly loaded into the hydrogel and released naturally. Most drugs are released in the early stages of injury repair. The formation of adhesive tissue occurs largely during the second stage of injury repair, which lasts from a few days to several weeks after the injury. This results in a relatively low drug content around the tendon during the peak period of adhesive

tissue formation, which is not conducive to the inhibition of fibrosis by the drug. In this study, by combining IM with a MOF, a ZIF-8 drug delivery system was utilized to slow the release time of IM and increase the content of IM in the peritendinous tissue during the peak period of collagen synthesis. This improves the efficacy of anti-adhesion drugs. Interestingly, by loading the ZIF-8 into the hydrogel, we found that its biomechanical strength was stronger than that of the pure hydrogel, and it has self-healing property, thus reducing the side effects caused by crushing the gel during the treatment process (Fig. S3). This can be explained by the mechanisms that hydrogels attached to the tendon are often crushed into a broken barrier under the pressure of the surrounding tissues and the drag force of tendon activity [40].

New anti-adhesion mechanisms and related anti-fibrotic drugs have also become a recent research hotspot [41]. Previously, the majority of anti-adhesion research had concentrated on transforming growth factor

β1 and the suppression of extracellular regulatory protein kinases and their downstream effectors [42]. Research on antifibrotic drugs is mostly limited to the effects of drugs on fibroblasts and myofibroblasts while neglecting the crucial impact on tendon stem cells during tendon healing. Therefore, in this study, we screened potential anti-fibrotic drugs and compared their inhibition levels on fibroblasts and tendon stem cells to select IM with relatively specific inhibition of fibroblast proliferation and a lower impact on tendon stem cells. To explore the mechanism by which IM inhibits fibrosis, we used second-generation sequencing to more accurately identify changes in various related molecules in fibroblasts after co-incubation with IM. Final localization significantly reduced the fibrosis-related factor CLDN1. At present, studies have found that CLDN1 regulated by the ERK/STAT3 pathway plays a crucial role in tumor pathology, with immune escape characteristics and fibrotic diseases that span multiple organs [43]. In this study, we confirmed that CLDN1 is closely related to the formation of adhesions. At the same time, the results of single-cell sequencing in human adhesive tissue showed that the expression of PDGFRβ was significantly increased in adhesive tissue and widely expressed in almost all fibroblasts. And after PDGFRβ was inhibited, the expression of CLDN1 was significantly reduced, as did the phosphorylation of ERK and STAT3. These results confirmed that CLDN1 plays a downstream role in PDGFRβ signaling. More specifically, in keloid fibrosis, IM inhibits the PDGFRβ/ERK/STAT3/CLDN1 signal transduction pathway and exerts an inhibitory effect on the formation of peritendinous adhesions. These findings shed light on the molecular processes that underlie peritendinous adhesion, novel targets, and associated anti-adhesion medications.

The discovery of novel medications offers insight into possible new ways to prevent and treat tendon adhesions. The combination of the drug-loaded MOF ZIF-8 and the hydrogel to form a better anti-adhesion sustained release hydrogel also brings some insights into traditional anti-adhesion materials.

Nevertheless, this study is subject to several limitations. Firstly, due to the limited amount of tissue fluid around the tendon, we were unable to detect specific pH changes in the tendon microenvironment at various time points during the repair process of normal tendon injuries. Consequently, we did not conduct detailed testing of the specific change curve of IM@ZIF-8@Gel release in the body. Secondly, in animal experiments, whether the specific amount of hydrogel wrapped around the tendon had a more optimal volume and the corresponding concentration of drug loading requires further research in the future. Thirdly, in this study, we chose the fibrosis-related molecule CLDN1 as our research focus on identifying new pathways for anti-tendon adhesion. However, whether other pathways play a role in the drug action process was not examined in this study. Further studies are required to comprehensively elucidate the mechanism by which IM inhibits cell adhesion.

4. Conclusions

IM was loaded through the ZIF-8 and mixed into the hydrogel. Subsequently, the study focused on investigating its inhibitory effects on proliferation, adhesion, and associated molecular pathways. The hydrogel loaded with ZIF-8 exhibited a sustained release of IM and high mechanical strength. *In vitro*, drug-loaded gels inhibited the proliferation, adhesion, and collagen secretion of myofibroblasts. *In vivo,* wrapping the hydrogel around the repaired tendon could prevent adhesion around the tendon through inhibition of the PDGFRβ/ERK/STAT3/CLDN1 pathway.

5. Experimental section

5.1. Synthesis of IM@ZIF-8

To synthesize IM@ZIF-8, 2.5 mL of iminib mesylate (IM) solution (2, 2.5, or 8 mg/mL) was stirred in 100 mL of Zn $(CH_3COO)_2 \cdot 2H_2O$ solution

(43.9 mg/mL) for 15 min. Then, 10 mL of 2-methylimidazole (0.12 g/mL) was added and stirred at 30 °C for 4 h to observe an opaque mixture. After centralization and washing with ethanol and H_2O sequentially, followed by free-drying, the precision was collected as IM@ZIF-8 with varying amounts of dry loading. Accordingly, ZIF-8 could also be prepared without drug addiction.

5.2. Synthesis of hydrogel

CEC polymer and OHA were dissolved separately in deionized water at a concentration of 2 % (wt/vol) each. The CEC solution and OHA solutions were blended at 37 °C to make the hydrogels and the molar ratio of CEC: OHA was set as 1:1.

5.3. Synthesis of IM@ZIF-8@Gel

The drug-loaded OHA/CEC hydrogels were prepared using a similar method to that employed for the synthesis of OHA/CEC hydrogels. Specifically, The 2 % (wt/vol) OHA solution was used to resolve the desired amounts of synthesized nanoparticles ahead. After that, the OHA solution with nanoparticle contents was mixed with 2 % (wt/vol) CEC solution at 37 °C (Fig. S2).

5.4. Research on material characteristics

The morphology of ZIF-8 and Gel was examined using scanning electron microscopy (SEM) under vacuum-dried conditions. The Nicolet-760 FITR spectrometer's attenuated total reflection mode was utilized to examine the chemical structure within the wavelength range of 4000 to 400 cm^{-1} (Fig. S5). The specimens were placed on a uniaxial testing apparatus (Instron 5567, Norwood, MA) equipped with a 50 N load cell, and subjected to a reduction in size at a rate of 10 mm per minute until Gel fracture occurred (Fig. S4). This methodology was employed for the analysis of elastic modulus.

5.5. Screening drugs

For our study, we utilized 208 F rat fibroblast cell lines (208 F s) and tendon-derived stem cells (TDSCs) as cellular models. A seeding density of 2×10^3 cells per well was established on a 64-well plate for both cell types. The TDSCs extraction was achieved by collecting only the mid substance of rat Achilles tendons, chopping the tissue, breaking it down into single cells with type I collagenase, and culturing it with a complete medium. The cells were cultured in DMEM supplemented with 10 % fetal bovine serum and 1 % antibiotics and were then incubated at 37 °C with a 5 % CO2 concentration. After one day, the cells were treated with ten drugs, including 10 μM of IM, for 24, 72, and 120 h, respectively. Subsequently, the samples were analyzed using Cell Counting Kit-8 as per the guidelines provided by the manufacturer. In short, Add the CCK8 culture medium mixture mixed in a 1:10 ratio to each sample in a 64-well plate and incubate for another 4 h. Next, proliferation determination was conducted by measuring the absorbance at 490 nm using a spectrophotometer (Synergy 2; BioTek, Winooski, VT). The result is expressed as the average absorbance value of each hole.

5.6. Investigate the mechanism of IM inhibition of fibroblasts

208 F cells were inoculated into a culture dish and placed in DMEM supplemented with 10 % fetal bovine serum and 1 % antibiotics, followed by incubation at 37 °C with a 5 % CO2 concentration. One day later, IM was added to a concentration of 10 μM, while the control group received an equal amount of PBS for Rna seq (Fig. S8).

5.7. Screening for optimal concentration

208 F and TDSC were inoculated into a culture dish and placed in

DMEM supplemented with 10 % fetal bovine serum and 1 % antibiotics, followed by incubation at 37 °C and 5 % CO$_2$ concentration. Before co-culturing with the release medium, TGF-β1 (10 ng/mL) was added to the 208 F culture medium and incubated for 24 h to fully activate it. Then, three concentrations of hydrogel and the extract of hydrogel containing only nanoparticles were collected for 7–14 days. These were co-cultured with fibroblasts and TDSC, and cell viability was assessed through CCK8 three days later.

5.8. Determination of IM release curve and hydrogel degradation curve

To assess the release behavior of IM from IM@ZIF-8@Gel and IM@Gel, the two groups of hydrogels were immersed in PBS adjusted to pH 7.4 and 6 to simulate release under neutral and acid conditions. They were then shaken at 37 °C. At each predetermined time point, the released solution was collected, and fresh PBS was added. The release rate (RR%) of IM was calculated by RR=(Wi/WTotal) * 100 %, where Wi is the amount of IM in the released solution and Wtotal is the total amount of IM. The release experiment was repeated in triplicate (Figs. S6 and S7a).

The initial weights of Gel and IM@ZIF-8@Gel were weighed and described as W0. Then, 1 mL hydrogels were immersed in 4 mL PBS with a pH of 6, placed in a shaker at 37 °C, and shaken at a speed of 60 rpm/min. At pre-set time intervals, hydrogels were taken out from PBS, and the water on the hydrogel surface was wiped off. Subsequently, the hydrogels were weighed to record their mass change over time. The weight of the hydrogel at pre-set time intervals was described as Wt. The mass change was calculated according to the following equation (Fig. S7b):

$$Mass\ change = Wt/W0$$

5.9. Single-cell RNA-Seq

The scRNA-Seq libraries were generated using the 10X Genomics Chromium Controller Instrument and Chromium Single Cell 3' V3.1 Reagent Kits (10X Genomics, Pleasanton, CA). Cells were concentrated to approximately 1000 cells/uL. Single-cell Gel Bead-In-Emulsions (GEMs) were generated by loading the cells into each channel. GEMs were subsequently ruptured by an RT step, followed by purification and amplification of the barcoded-cDNA. The amplified barcoded cDNA was fragmented, A-tailed, ligated with adaptors, and index PCR amplified. The final libraries were quantified using the Qubit High Sensitivity DNA assay (Thermo Fisher Scientific) and the size distribution of the libraries was determined using a High Sensitivity DNA chip on a Bioanalyzer 2200 (Agilent). Lastly, all libraries were sequenced on an Illumina sequencer (Illumina, San Diego, CA) using a 150 bp paired-end run (Fig. S9).

5.10. Cell experiments

Immerse IM@ZIF-8@Gel, IM@Gel, ZIF-8@Gel, and Gel into PBS respectively, adjusting the pH to 6, and shaking them at 37 °C. Collect solutions released in 7–14 days. Following the filtration of bacteria, the hydrogel extracts from the four groups were diluted in a certain proportion with the complete culture medium and then co-cultured with the cultured cells. The control group is supplemented with an equal volume of solvent.

5.11. In vitro cell adhesion experiment

The cell adhesion test was determined by observing the arrangement of the cytoskeleton through actin staining on the 3rd day after incubation. 208 F cells were seeded onto a 24-well plate and cultured in the aforementioned medium. Following a 3-day incubation period, cells were fixed with a 4 % paraformaldehyde solution for 10 min.

Subsequently, they were submerged in a 10-min bath of 0.1 % Triton X-100 (Sigma Aldrich), followed by repeated rinsing with PBS at room temperature. Following the manufacturer's protocol, cells were stained with Perform Abcam staining solution at a concentration of 20 μg/mL. After a 5-min DAPI staining with a concentration of 1 μg/mL, the specimens were examined using confocal laser scanning microscopy (Leica TCS SP2; Leica Microsystems, Heidelberg, Germany) and analyzed using NIH image J imaging software. The results are represented as the average diffusion area of myofibroblasts on each surface.

5.12. In vitro proliferation inhibition experiment

208 F was cultured on a 64-well plate using the aforementioned culture medium until reaching the 1st, 3rd, and 5th days, followed by analysis using Cell Counting Kit-8 8 according to the manufacturer's instructions. In short, a mixture of CCK-8 and culture medium in a 1:10 ratio was added to each sample in a 64-well plate and incubated for another 4 h. The absorbance at 490 nm was then measured using a spectrophotometer to determine proliferation (Synergy 2; BioTek, Winooski, VT). The result is expressed as the average absorbance value of each well.

5.13. Determination of cell activity

208 F was cultured on a 64-well plate with the aforementioned medium until the 3rd day, followed by cell activity assessment using a staining kit. The results were detected using a fluorescence microscope. The results are presented as the proportion of deceased cells relative to viable cells per well.

5.14. In vitro cell protein expression\

Western blot was performed as described previously [44,45]. The expression of Col III, ERK1/2, p-ERK1/2, STAT3, p-STAT3, and CLDN1 was assessed through Western blotting, with β-actin serving as an internal control. The following primary antibodies were used: anti-Col III (1:1000), anti-ERK1/2 (1:500), anti-p-ERK1/2 (1:1000), anti-STAT3 (1:1000), anti-p-STAT3 (1:1000), and CLDN1 (1:500). β-Actin (1:10,000) was used as an internal control. Protein visualization and image capture were performed using an automated chemiluminescence imaging analysis system. Protein expression levels were quantified using ImageJ software (Fig. S10).

5.15. Animal experiments

Sprague Dawley rats weighing between 200 and 250 g were chosen as the animal model. All animal research protocols were conducted in compliance with the policies of the School of Medicine of Shanghai Jiao Tong University. Specifically, the rats in the experiment were given an intravenous injection of pentobarbital sodium to help them anesthetize (30 mg/kg body weight), followed by disinfection of their hind limbs to establish a model of tendon sheath adhesion. The Achilles tendon was then cut through the posterior middle skin incision in a transverse manner. Subsequently, the tendon was mended with an improved Kessler tendon suture. The rats were randomly divided into five groups (n = 12 per group): 1 mL IM@ZIF-8@Gel, IM@Gel, ZIF-8@Gel, and Gel were wrapped around the repair site of the Achilles tendon, and the rats not wrapped with hydrogel around the tendon were used as controls (Fig. S12).

5.16. Macro evaluation

Three weeks post-surgery, the hind limbs were examined for signs of inflammation or ulcers. Subsequently, the repair site was opened to evaluate tendon sheath adhesion by direct observation of the Achilles tendon surgical site. Specifically, levels 1–5 are classified according to

the adhesion scoring system: Level 1, the tendon does not have any adhesive tissue on its surface; Level 2, The tendon may not have as much adhesive tissue on its surface; then, it is relatively easy to detach it from the tendon with a blunt touch; Level 3, ≤50 % of areas with adhesive tissue can be divided by blunt instead of sharp tools; Level 4, 51–97.5 % of the area is attached with adhesive tissue that can be quickly released and separated; At level 5, 97.5 % of the areas have adhesive tissue that can be quickly released and separated (Fig. S13).

5.17. Organizational evaluation

Three weeks post-surgery, the extracted tendons were labeled with hematoxylin-eosin (H&E) and Masson trichrome staining. The levels of adhesion at the surgical sites was assessed on a scale of 1–5 (Fig. S14). The levels of healing at the surgical sites were evaluated on a scale of 1–4 (Fig. S15).

5.18. Tendon mechanics testing

To investigate whether the drug-loaded gel hindered the tendon healing process, the maximum tensile strength of the repaired tendon was recorded (Fig. S11).

5.19. Protein expression in peritendinous tissue

Immunohistochemical staining of Col III, Col I and CLDN1 were performed on five groups of samples to evaluate their expression in the peritendon area (Fig. S17). Additionally, the expression of related genes was further confirmed through Western blot analysis (Fig. S16).

5.20. Statistical analysis

All values are presented as the mean $\pm$ standard deviation (SD). Statistical analysis was conducted using Student's t-test to compare the two groups. For multiple comparisons, one-way analysis of variance and Fisher's exact tests were utilized. In this study, a p-value <0.05 was considered indicative of a significant difference.

Ethics approval and consent to participate

All animal procedures were approved by institutional review committee of Shanghai. Jiao Tong University (SYXK (Hu)2021–0028).

The collection of tissue samples from all patients was approved by the Medical Ethics Committee of Wuxi Ninth People's Hospital (KT201803).

CRediT authorship contribution statement

Sa Pang: Writing – original draft, Methodology, Data curation, Conceptualization. **Rongpu Wu:** Validation, Methodology, Data curation, Conceptualization. **Wenxin Lv:** Writing – original draft, Methodology. **Jian Zou:** Writing – review & editing, Funding acquisition. **Yuange Li:** Validation. **Yanhao Li:** Validation. **Peilin Zhang:** Methodology, Conceptualization. **Xin Ma:** Writing – review & editing, Resources, Funding acquisition. **Yi Wang:** Project administration, Funding acquisition, Conceptualization. **Shen Liu:** Writing – review & editing, Investigation, Funding acquisition, Conceptualization.

Declaration of competing interest

The authors declare no conflict of interest.

Acknowledgements

Appendix A. Supplementary data

Supplementary data to this article can be found online at https://doi.org/10.1016/j.bioactmat.2024.04.012.

References

[1] P.B. Voleti, M.R. Buckley, L.J. Soslowsky, Tendon healing: repair and regeneration, Annu. Rev. Biomed. Eng. 14 (2012) 47–71.

[2] P. Sharma, N. Maffulli, Biology of tendon injury: healing, modeling and remodeling, J. Musculoskelet. Neuronal Interact. 6 (2) (2006) 181–190.

[3] H. Zhou, H. Lu, Advances in the development of anti-adhesive biomaterials for tendon repair treatment, Tissue Eng. Regen Med. 18 (1) (2021) 1–14.

[4] C. Cai, et al., MMP-2 responsive unidirectional hydrogel-electrospun patch loading TGF-β1 siRNA polyplexes for peritendinous anti-adhesion, Adv. Funct. Mater. 31 (6) (2020).

[5] Y. Kaneti, et al., Strategies for improving the functionality of zeolitic imidazolate frameworks: tailoring nanoarchitectures for functional applications, Adv. Mater. 29 (38) (2017).

[6] N. Soomro, et al., Natural drug physcion encapsulated zeolitic imidazolate framework, and their application as antimicrobial agent, Colloids Surf. B Biointerfaces 182 (2019) 110364.

[7] Q. Wang, et al., Synthesis and modification of ZIF-8 and its application in drug delivery and tumor therapy, RSC Adv. 10 (62) (2020) 37600–37620.

[8] H. Zheng, et al., One-pot synthesis of metal-organic frameworks with encapsulated target molecules and their applications for controlled drug delivery, J. Am. Chem. Soc. 138 (3) (2016) 962–968.

[9] Maryam Chafiq, et al., Recent advances in multifunctional reticular framework nanoparticles: a paradigm shift in materials science road to a structured future, Nano-Micro Lett. 15 (1) (2023) 213.

[10] G. Meier Bürgisser, J. Buschmann, History and performance of implant materials applied as peritendinous antiadhesives, J. Biomed. Mater. Res. B Appl. Biomater. 103 (1) (2015) 212–228.

[11] Jun Chen, et al., MOFs-based nitric oxide therapy for tendon regeneration, Nano-Micro Lett. 13 (1) (2020) 23.

[12] J. Wong, et al., The cellular biology of flexor tendon adhesion formation: an old problem in a new paradigm, Am. J. Pathol. 175 (5) (2009) 1938–1951.

[13] Y. Zhang, et al., P120-catenin regulates pulmonary fibrosis and TGF-β induced lung fibroblast differentiation, Life Sci. 230 (2019) 35–44.

[14] L. van Steensel, et al., Imatinib mesylate and AMN107 inhibit PDGF-signaling in orbital fibroblasts: a potential treatment for Graves' ophthalmopathy, Invest. Ophthalmol. Vis. Sci. 50 (7) (2009) 3091–3098.

[15] W. Su, Y. Chen, F. Lin, Injectable oxidized hyaluronic acid/adipic acid dihydrazide hydrogel for nucleus pulposus regeneration, Acta Biomater. 6 (8) (2010) 3044–3055.

[16] Z. Xu, et al., Intra-articular platelet-rich plasma combined with hyaluronic acid injection for knee osteoarthritis is superior to platelet-rich plasma or hyaluronic acid alone in inhibiting inflammation and improving pain and function, Arthroscopy : J. Arthroscopic & Related Surg. : Off. Publ. Arthroscopy Assoc. North Am. Int. Arthroscopy Assoc. 37 (3) (2021) 903–915.

[17] J. Burdick, G. Prestwich, Hyaluronic acid hydrogels for biomedical applications, Adv. Mater. 23 (12) (2011) H41–H56.

[18] M. Karaaltin, et al., The effects of 5-fluorouracil on flexor tendon healing by using a biodegradable gelatin, slow releasing system: experimental study in a hen model, J. Hand Surg. 38 (6) (2013) 651–657. European volume.

[19] J. Li, D. Mooney, Designing hydrogels for controlled drug delivery, Nat. Rev. Mater. 1 (12) (2016).

[20] J. Qu, et al., Degradable conductive injectable hydrogels as novel antibacterial, anti-oxidant wound dressings for wound healing, Chem. Eng. J. 362 (2019) 548–560.

[21] Y. Xiong, Z. Zhang, Zhongguo xiu fu chong jian wai ke za zhi 20 (3) (2006) 251–255.

[22] J.A. Creech-Organ, S.E. Szybist, J.L. Yurgil, Joint and soft tissue injections, Am. Fam. Physician 108 (2) (2023) 151–158.

[23] A. Rouhani, A. Tabrizi, E. Ghavidel, Effects of non-steroidal anti-inflammatory drugs on flexor tendon rehabilitation after repair, Arch. Bone Jt. Surg. 1 (1) (2013) 28–30.

[24] G. Meier Bürgisser, J. Buschmann, History and performance of implant materials applied as peritendinous antiadhesives, J. Biomed. Mater. Res. B Appl. Biomater. 103 (1) (2015) 212–228.

[25] C.F. Waller, Imatinib mesylate, Recent Results Cancer Res. 212 (2018) 1–27.

[26] C.E. Daniels, M.C. Wilkes, M. Edens, et al., Imatinib mesylate inhibits the profibrogenic activity of TGF-beta and prevents bleomycin-mediated lung fibrosis, J. Clin. Invest. 114 (9) (2004) 1308–1316.

[27] W.L. Kuo, M.C. Yu, J.F. Lee, C.N. Tsai, T.C. Chen, M.F. Chen, Imatinib mesylate improves liver regeneration and attenuates liver fibrogenesis in CCL4-treated mice, J. Gastrointest. Surg. 16 (2) (2012) 361–369.

[28] J.H. Distler, A. Jüngel, L.C. Huber, et al., Imatinib mesylate reduces production of extracellular matrix and prevents development of experimental dermal fibrosis, Arthritis Rheum. 56 (1) (2007) 311–322.

[29] J. Wong, et al., The cellular biology of flexor tendon adhesion formation: an old problem in a new paradigm, Am. J. Pathol. 175 (5) (2009) 1938–1951.

[30] S.A. Pot, Z. Lin, J. Shiu, M.C. Benn, V. Vogel, Growth factors and mechano-regulated reciprocal crosstalk with extracellular matrix tune the keratocyte-fibroblast/myofibroblast transition, Sci. Rep. 13 (1) (2023) 11350, https://doi.org/10.1038/s41598-023-37776-9. Published 2023 Jul 13.

[31] W. Su, Y. Chen, F. Lin, Injectable oxidized hyaluronic acid/adipic acid dihydrazide hydrogel for nucleus pulposus regeneration, Acta Biomater. 6 (8) (2010) 3044–3055.

[32] Z. Xu, et al., Intra-articular platelet-rich plasma combined with hyaluronic acid injection for knee osteoarthritis is superior to platelet-rich plasma or hyaluronic acid alone in inhibiting inflammation and improving pain and function, Arthroscopy : J. Arthroscopic & Related Surg. : Off. Publ. Arthroscopy Assoc. North Am. Int. Arthroscopy Assoc. 37 (3) (2021) 903–915.

[33] J. Burdick, G. Prestwich, Hyaluronic acid hydrogels for biomedical applications, Adv. Mater. 23 (12) (2011) H41–H56.

[34] M. Karaaltin, et al., The effects of 5-fluorouracil on flexor tendon healing by using a biodegradable gelatin, slow releasing system: experimental study in a hen model, J. Hand Surg., European 38 (6) (2013) 651–657.

[35] J. Li, D. Mooney, Designing hydrogels for controlled drug delivery, Nat. Rev. Mater. 1 (12) (2016).

[36] J. Qu, et al., Degradable conductive injectable hydrogels as novel antibacterial, anti-oxidant wound dressings for wound healing, Chem. Eng. J. 362 (2019) 548–560.

[37] J.W. Howell, F. Peck, Rehabilitation of flexor and extensor tendon injuries in the hand: current updates, Injury 44 (3) (2013) 397–402.

[38] J. Li, X. Feng, B. Liu, et al., Polymer materials for prevention of postoperative adhesion, Acta Biomater. 61 (2017) 21–40.

[39] C. Cai, X. Zhang, Y. Li, et al., Self-healing hydrogel embodied with macrophage-regulation and responsive-gene-silencing properties for synergistic prevention of peritendinous adhesion, Adv. Mater. 34 (5) (2022) e2106564.

[40] B.R. Freedman, D.J. Mooney, Biomaterials to mimic and heal connective tissues, Adv. Mater. 31 (19) (2019) e1806695.

[41] Q. Hu, X. Xia, X. Kang, et al., A review of physiological and cellular mechanisms underlying fibrotic postoperative adhesion, Int. J. Biol. Sci. 17 (1) (2021) 298–306. Published 2021 Jan 1.

[42] G. Wu, B. Sun, C. Zhao, et al., Three-dimensional tendon scaffold loaded with TGF-β1 gene silencing plasmid prevents tendon adhesion and promotes tendon repair, ACS Biomater. Sci. Eng. 7 (12) (2021) 5739–5748.

[43] N. Roehlen, A. Saviano, H. El Saghire, et al., A monoclonal antibody targeting nonjunctional claudin-1 inhibits fibrosis in patient-derived models by modulating cell plasticity, Sci. Transl. Med. 14 (676) (2022) eabj4221.

[44] X. Liu, Y. Gu, S. Kumar, et al., Oxylipin-PPARγ-initiated adipocyte senescence propagates secondary senescence in the bone marrow, Cell Metabol. 35 (4) (2023), 667-684.e6.

[45] X. Liu, Y. Chai, G. Liu, et al., Osteoclasts protect bone blood vessels against senescence through the angiogenin/plexin-B2 axis, Nat. Commun. 12 (1) (2021) 1832. Published 2021 Mar 23.